Modeling of Sparsely Sampled Tubular Surfaces Using Coupled Curves

Thorsten Schmidt[1,2], Margret Keuper[1,2], Taras Pasternak[3], Klaus Palme[1,3,4] and Olaf Ronneberger[1,2]

[1]Lehrstuhl für Mustererkennung und Bildverabeitung, Institut für Informatik,
[2]Centre of Biological Signalling Studies (BIOSS),
[3]Institut für Biologie II, [4]Freiburg Inst. for Advanced Studies (FRIAS),
Albert-Ludwigs-Universität Freiburg
tschmidt@informatik.uni-freiburg.de

Abstract. We present a variational approach to simultaneously trace the axis and determine the thickness of 3-D (or 2-D) tubular structures defined by sparsely and unevenly sampled noisy surface points. Many existing approaches try to solve the axis-tracing and the precise fitting in two subsequent steps. In contrast to this our model is initialized with a small cylinder segment and converges to the final tubular structure in a single energy minimization using a gradient descent scheme. The energy is based on the error of fit and simultaneously penalizes strong curvature and thickness variations. We demonstrate the performance of this closed formulation on volumetric microscopic data sets of the *Arabidopsis* root tip, where only the nuclei of the cells are visible.

1 Introduction

The accurate tracing and segmentation of parallel-line (2D) or tubular structures (3D) is an active research topic to solve problems coming from medicine, biology, robotics, or aerial and satellite image analysis. Especially for biological and medical applications, with their wide spectrum of imaging methods this modeling is an important step towards data abstraction and quantification. With the discovery of the green fluorescent protein, and the isolation of its gene, the possibility of imaging organism development in-vivo has led to a revolution in biological research and a tremendous increase in data volume to process.

One popular model organism in plant science is *Arabidopsis thaliana*, due to its simple architecture and comparably small and fully sequenced genome. Especially the stem cell niches in the root and shoot tips (root/shoot apical meristems) are of high interest to understand plant development and signaling within complex organs. The root apical meristem (RAM) consists of a set of tissue layers around the root's axis. Each of these layers can be described using an axis-thickness model, leading to the continuous anatomical model needed to localize events within the root. The simplest and most flexible way of imaging the plant root with cellular resolution is to mark the cell nuclei and relate events within the organs to a derived overall anatomical model. However, this practical

imaging advantage leads to a very sparse representation of the coaxial tubular structures each cell layer represents, posing high demands onto the modeling.

Especially in microscopic data the light is attenuated by the specimen density and scattered at interfaces between regions with different refractive indices leading to a significant loss of signal when imaging through thick tissues. Therefore simple gray-value based approaches like thresholding and/or kernel smoothing to estimate the root axis are biased towards the part of the root close to the objective and tend to fail. We therefore avoid direct use of the image gray values, and instead extract the positions of the nuclei of a selected layer using the detection scheme described in [10]. The detection quality is also biased due to the described effects, and a direct fit to the resulting point cloud using kernel smoothing still shows a systematic fitting error as we will show in the experiments section.

To avoid the described bias we employed a model consisting of a vector-valued function describing the tube's axis and a scalar function describing the variable tube thickness. Both functions are coupled by a common curve parametrization into a combined tubular model which is fit to the data in a robust variational energy minimization scheme. The model is designed to work solely on the sparse point positions, without the need for surface normal estimation. We will show that it leads to very accurate fits even in the case of high noise and missing surface points.

A key benefit of the proposed model is that it "grows" into a large and arbitrarily complex tubular structure from a small local initialization, i.e. it solves the tracing and accurate fitting problem within a single energy minimization.

1.1 Related Work

In medical applications various approaches exist to analyze images of vascular and neuronal networks based on different imaging methods ranging from low resolution CT and MRT, through light microscopy down to electron microscopy [7, 3]. All approaches have in common that they rely on densely imaged interfaces between the structures of interest and mainly depend on the gray values and their derivatives to guide the model fitting. One possibility of robustly finding the axis of a tubular structure is a symmetry analysis around the potential axis [8]. Morphology-driven approaches try to find the axis by structure thinning leading to a skeletonization. Filter based approaches first try to emphasize the structures using filter banks or steerable filters and apply thresholding and thinning afterwards. See [4] for an overview comparing the different approaches.

In the field of robotics approaches to fit parametric tubular structures to point cloud data recorded using laser range scanners are of high interest [1]. Most existing approaches exploit the scanned dense mesh structure to estimate local surface normals guiding the model fitting process. These approaches have to cope with noisy data and therefore estimate the normals for each surface position from relatively large neighborhoods. Others try to detect shapes using Hough-like voting based approaches [9]. These are especially suited to detect man-made rigid objects, but don't perform well on deformable objects as they are common in biological and medical applications.

In [5] the coupling of two evolving splines describing the center-lines and thicknesses of roads and rivers in aerial and satellite images was introduced. Although the noise level in images of that kind is very high, the gradients are still a valuable piece of information to guide the snake evolution. A different approach using two coupled splines to describe the outlines of the biologically highly interesting model organism C-Elegans was introduced in [11].

In [6] a non-self-intersecting 1-D line from unstructured and noisy 3D point data was reconstructed using moving least-squares interpolation. For homogeneously distributed tube-surface data around its circumference this approach is also applicable to solve the tube axis fitting task, although it does not determine the tube thickness.

Our setting is different from the above-mentioned, since our approach has to perform the task of simultaneously estimating the axis and variable thickness of a tubular structure based on sparse surface points only. The low point density and high data noise preclude the extraction of reliable surface normals. We formulate the task of fitting the model to a point cloud as one closed energy minimization problem, which incorporates all available points and a set of tubular models to which on demand new tubes can be added.

2 Variational Coupled Curve Fitting

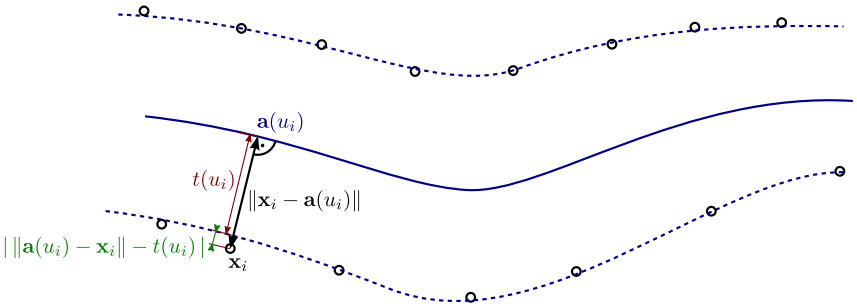

Fig. 1. A 2-D sketch of the tube model fit to a point set depicted as black circles. The axis is shown as blue line, while the dashed lines indicate the estimated tube incorporating the tube thickness. The distance shown in green is minimized during the optimization.

We define a tube as a function mapping a curve parameter $u \in \mathbb{R}$ to the $(D+1)$-dimensional vector $\left(\boldsymbol{a}^\top(u), t(u)\right)^\top$, where $\boldsymbol{a} : \mathbb{R} \to \mathbb{R}^D$ is the tube axis function and $t : \mathbb{R} \to \mathbb{R}$ is the corresponding tube thickness function. Fig. 1 sketches the tube model. To optimally map the model to a set of tube surface

points $X = \{\boldsymbol{x}_1, \ldots, \boldsymbol{x}_n\}$, $\boldsymbol{x}_i \in \mathbb{R}^D$ we minimize the energy

$$E_{\text{data}}(\boldsymbol{a}, t) := \sum_{i=1}^{n} \psi\left(\left(\|\boldsymbol{a}(u_i) - \boldsymbol{x}_i\| - t(u_i) \right)^2 \right) \tag{1}$$

where $u_i := \arg\min_u \|\boldsymbol{x}_i - \boldsymbol{a}(u)\|$ is the curve parameter projection of $\boldsymbol{x}_i$ and $\psi\left(\rho^2\right)$ is a robust distance measure.

To cope with sparse surface points and high data noise, we additionally introduce smoothness terms penalizing axis curvature and tube thickness variations

$$E_a(\boldsymbol{a}) = \int_{-\infty}^{\infty} \left\| \frac{\mathrm{d}^2}{\mathrm{d}u^2} \boldsymbol{a}(u) \right\|^2 \mathrm{d}u \quad \text{and} \quad E_t(t) = \int_{-\infty}^{\infty} \left(\frac{\mathrm{d}}{\mathrm{d}u} t(u) \right)^2 \mathrm{d}u \,. \tag{2}$$

For shorter notation we define $\rho_i(u) := (\|\boldsymbol{a}(u) - \boldsymbol{x}_i\| - t(u))$ and get the overall energy functional to minimize

$$E(\boldsymbol{a}, t) := \sum_{i=1}^{n} \psi\left(\rho^2\right) + \lambda \int_{-\infty}^{\infty} \left\| \frac{\mathrm{d}^2}{\mathrm{d}u^2} \boldsymbol{a}(u) \right\|^2 \mathrm{d}u + \mu \int_{-\infty}^{\infty} \left(\frac{\mathrm{d}}{\mathrm{d}u} t(u) \right)^2 \mathrm{d}u \tag{3}$$

where $\lambda, \mu \in \mathbb{R}^+$ weigh the influence of the smoothness terms.

3 Parametrization Using B-Splines

We approximate the curves with open B-splines of degree p, therefore the nodes at the spline endpoints are repeated $p+1$ times. W.l.o.g. we will restrict the spline parameter u to the $[0, 1]$-range. We obtain the B-spline approximation of the general functions $\boldsymbol{a}(u)$ and $t(u)$ as follows:

$$\boldsymbol{a}(u) := \sum_{j=0}^{m-1} \boldsymbol{c}_j^a b_{j,p,\boldsymbol{s}}(u) \qquad \text{and} \qquad t(u) := \sum_{j=0}^{m-1} c_j^t b_{j,p,\boldsymbol{s}}(u)$$

where $C^a = \left\{\boldsymbol{c}_0^a, \ldots, \boldsymbol{c}_{m-1}^a\right\}$ and $C^t = \left\{c_0^t, \ldots, c_{m-1}^t\right\}$ are the control points, and $b_{j,p,\boldsymbol{s}}$ are the basis functions with node-vector $\boldsymbol{s} = (s_0, \ldots, s_{m+p})^\top$.

Lemma 1 (B-spline derivative). *Let $f(u) := \sum_{j=0}^{m-1} c_j b_{j,p,\boldsymbol{s}}(u)$ be a B-spline of degree $p \in \mathbb{N}_0$, with control points c_j, $j = 0, \ldots, m-1$ defined over the knot vector $\boldsymbol{s} = (s_0, \ldots, s_{m+p})^\top$. Then the derivative*

$$f'(u) = \frac{\mathrm{d}}{\mathrm{d}u} f(u) = \sum_{j=0}^{m-2} c'_j b_{j,p-1,\boldsymbol{s}'}(u)$$

is another B-spline of degree $p-1$ defined over the knot vector $s' = (s_1, \ldots, s_{m+p-1})$ with control points $c'_j = \frac{p}{s_{j+p+1} - s_{j+1}} (c_{j+1} - c_j)$.

More details to splines as well as this Lemma and its proof are detailed in [2].

The general energy from (3) changes to

$$\begin{aligned} E_{\text{data}}(\boldsymbol{a}, t) = \sum_{i=1}^{n} \psi\left(\left(\|\boldsymbol{a}(u_i) - \boldsymbol{x}_i\| - t(u_i) \right)^2 \right) \\ + \lambda \cdot \sum_{d=1}^{D} \int_0^1 \left(\sum_{j=0}^{m-3} c'^{a}_{j,d} b_{j,p-2,\boldsymbol{s}'}(u) \right)^2 \mathrm{d}u \\ + \mu \cdot \int_0^1 \left(\sum_{j=0}^{m-2} c'^{t}_{j} b_{j,p-1,\boldsymbol{s}'}(u) \right)^2 \mathrm{d}u \,. \end{aligned} \tag{4}$$

The primed variables are obtained applying Lemma 1 (for the axis twice) to the original splines.

Using the spline parameterization the partial derivatives with respect to the control points $\boldsymbol{c}^a_j$ and c^t_j are needed

$$\begin{aligned} \frac{\partial}{\partial c^a_{j,d}} E(\boldsymbol{a}, t) = 2 \sum_{i=1}^{n} \psi'\left(\rho^2\right) \left(1 - \frac{t(u_i)}{\|\boldsymbol{a}(u_i) - \boldsymbol{x}_i\|} \right) \left(a_d(u_i) - x_{i,d} \right) b_{j,p,\boldsymbol{s}}(u_i) \\ + 2\lambda \sum_{j'=0}^{m-1} c^a_{j',d} \int_0^1 \frac{\mathrm{d}^2}{\mathrm{d}u^2} b_{j',p,\boldsymbol{s}}(u) \frac{\mathrm{d}^2}{\mathrm{d}u^2} b_{j,p,\boldsymbol{s}}(u) \, \mathrm{d}u \end{aligned} \tag{5}$$

$$\begin{aligned} \frac{\partial}{\partial c^t_j} E(\boldsymbol{a}, t) = -2 \sum_{i=1}^{n} \psi'\left(\rho^2\right) \left(\|\boldsymbol{a}(u_i) - \boldsymbol{x}_i\| - t(u_i) \right) b_{j,p,\boldsymbol{s}}(u_i) \\ + 2\mu \sum_{j'=0}^{m-1} c^t_{j'} \int_0^1 \frac{\mathrm{d}}{\mathrm{d}u} b_{j',p,\boldsymbol{s}}(u) \frac{\mathrm{d}}{\mathrm{d}u} b_{j,p,\boldsymbol{s}}(u) \, \mathrm{d}u \,, \end{aligned} \tag{6}$$

finally leading to the following update rules for moving the control points in a gradient descent manner when introducing an artificial discrete evolution time k with step $\tau \in \mathbb{R}^+$:

$$c^{a\,k+1}_{j,d} = c^{a\,k}_{j,d} - \tau \frac{\partial}{\partial c^a_{j,d}} E(\boldsymbol{a}, t) \quad \text{and} \quad c^{t\,k+1}_{j} = c^{t\,k}_{j,d} - \tau \frac{\partial}{\partial c^t_j} E(\boldsymbol{a}, t) \,. \tag{7}$$

Since all dimensions come into play during the control point updates in each iteration, first the derivatives are computed for each control point, then the update is applied and finally the u_i for each point are recomputed.

We define the outlier-robust distance measure

$$\psi\left(\rho^2\right) := \begin{cases} \rho^2 & \rho < \eta \\ \eta^2 & \rho \geq \eta \end{cases} \qquad \text{with derivative} \qquad \psi'\left(\rho^2\right) = \begin{cases} 1 & \rho < \eta \\ 0 & \rho \geq \eta \end{cases}$$

and some user-defined threshold $\eta \in \mathbb{R}$ (which should be chosen in the range of the structure radius).

Algorithm 1 The Coupled B-spline fitting algorithm

Require: Point set X, initial cylinder, parameters λ, μ, τ
1: Initialize each model $(\boldsymbol{a}, t)$ with two knots fitting the initial cylinder
2: Compute the initial model energy $E(\boldsymbol{a}, t)$ using (4)
3: **while** not converged **do**
4: Minimize $E(\boldsymbol{a}, t)$ using (7)
5: Insert knot and re-parametrize the model
6: **end while**
7: **return** The coupled B-spline model $(\boldsymbol{a}, t)$

Only points within a certain distance range defined by η will contribute to the derivatives which allows to adapt the model fitting to the surface point density and the data noise. We additionally linearly decrease λ and μ with increasing arc length of the current axis estimate to avoid a bias towards short curves and update the thickness function only with points mapping orthogonally onto the axis to avoid a thickness over-estimation at the tube end points.

We initialize the fit with a manually chosen short cylinder segment represented by a straight B-spline with two knots at the ends with the thickness intialized to the cylinder radius. During the described optimization the number of control points remains constant. Therefore the model will evolve until no more data points can be described by one single degree p polynomial. To allow more complex tube shapes, we alternate between fitting and re-gridding step in which an additional knot is inserted and distribute the knots equidistantly along the curve leading to an intermediate curve length parametrization. The whole fitting process is described in Alg. 1.

3.1 Extension to Multiple Tubes

To simultaneously trace multiple tubular structures, for each a seeding cylinder can be placed. In each iteration step the point set is partitioned into subsets, so that the points in subset X_m are best explained by the mth tubular model according to the data energy term. The evolution of tube m is computed on subset X_m only. The Energy then becomes the sum over all single model Energies.

4 Experiments

4.1 Synthetic Data

We compared the proposed model (using cubic splines) to the axis estimates obtained through Gaussian point cloud kernel smoothing (PKS), which resembles the drawbacks of averaging techniques for curve fitting. For this we synthetically generated data sets consisting of point clouds highlighting specific cases. We used trigonometric functions to model the axis and thickness functions and generated 1000 equally distributed tube surface points around the axis. The point positions were then moved in an arbitrary direction following a Gaussian distribution with

standard deviation σ leading to the synthetic ground truth (Fig. 2 left panels). The PKS kernel width was empirically chosen to minimize the fitting error. The error comparison between PKS and the proposed coupled curve model (CCM) is shown in the right panels. For constant tube thickness Fig. 2(a) the axis error of CCM in each direction stays below 20% of the tube thickness whereas PKS already over-smooths the curve leading to undershoots. The thickness is a little over-estimated by on average 5%. Pure thickness variations as in Fig. 2(b) do not influence the axis localization accuracy, but they are reflected in the thickness error, because the model is designed to favor a constant thickness. However, the error stays below 10% for low noise and small μ (here $\mu = 0$). Moderate thickness variations on a bent model as shown in Fig. 2(c) affect the quality of fit only marginally. Finally one of the big strengths of the model is highlighted in

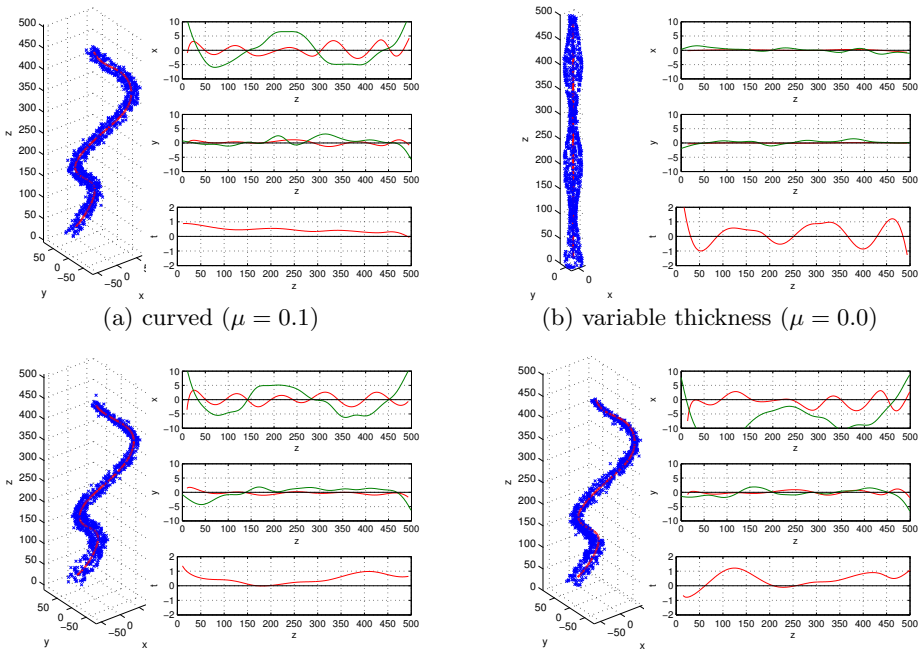

(a) curved ($\mu = 0.1$) (b) variable thickness ($\mu = 0.0$)

(c) curved + var. thickness ($\mu = 0.1$) (d) "self-occlusion" ($\mu = 0.1$)

Fig. 2. Sample fits to synthetically generated tubes and the fitting errors for each model dimension ($u = [0, 500]$). The left plots show the generated noisy point clouds (blue crosses) and the axis estimate using the proposed coupled curves model (CCM). The right plots show the axis mismatch in $x-$ and $y-$ direction for point based kernel smoothing (PKS) in green and for the CCM in red. The third plot shows the CCM thickness mismatch. For all experiments we set $\lambda = 0.1$. (a) $\boldsymbol{a}(u) = (50\sin(2\pi u/300), 70\sin(2\pi u/800), u)^\top$, $t(u) = 10$, $\sigma = 4$; (b) $\boldsymbol{a}(u) = (0, 0, u)^\top$, $t(u) = 20+10\sin(2\pi u/200)$, $\sigma = 1$; (c) $\boldsymbol{a}(u) = (50\sin(2\pi u/300), 70\sin(2\pi u/800), u)^\top$, $t(u) = 10+5\sin(2\pi u/1000)$, $\sigma = 4$; (d) $\boldsymbol{a}(u) = (50\sin(2\pi u/300), 70\sin(2\pi u/800), u)^\top$, $t(u) = 10 + 5\sin(2\pi u/1000)$, $\sigma = 4$, with "self-occlusion"

Fig. 2(d), the robustness to biased point cloud distributions on the tube surface. For this all sample points from Fig. 2(c) which are occluded when assuming a solid tube and a fixed view angle were removed from the set. This resulted in an axis position bias for PKS, whereas CCM still reliably estimates tube localization and thickness.

4.2 Microscopic 3D Volumes of the *Arabidopsis* Root Tip

To highlight the practical applicability and robustness of our approach we estimated axis and thickness of *Arabidopsis* root tips using the cell nuclei. The root tips were fixated and DAPI stained to mark the cellular DNA content. After preparation they were recorded using a confocal laser scanning microscope (CLSM) with a 63× water immersion objective. The data volume was reconstructed from a sequence of images using optical sectioning, leading to a final anisotropic voxel-size of $0.2\mu m$ in lateral (x-y) and $1\mu m$ in axial (z) direction. Two orthogonal views of a sample root with superimposed axis fits are shown in

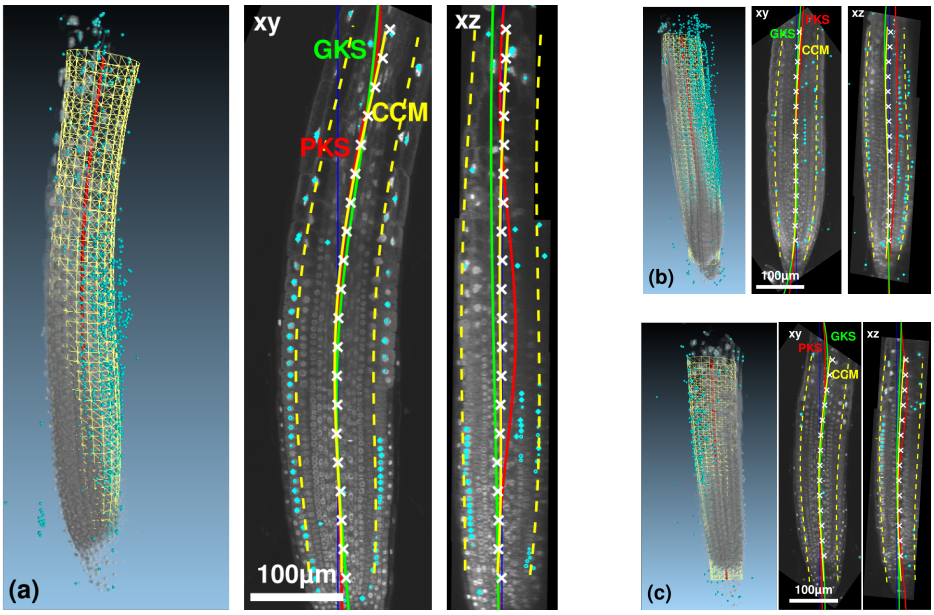

Fig. 3. The Coupled Curves model fit to sample root tip data sets. In gray the gamma corrected DAPI signal is shown, the red line (left panels) depicts the estimated root axis, the yellow mesh the estimated center of the epidermal cell layer and the cyan spheres the noisy epidermis nucleus positions. The right panels show orthogonal cuts through the data sets and the axis fits using gray-value-based kernel smoothing (GKS), point-based kernel smoothing (PKS) and the proposed Coupled Curve Model (CCM). The blue line indicates the cut shown in the different views. One expert annotation is shown as white crosses. The parameters for the CCM model were set to $\lambda = 0.1,\ \mu = 0.1$.

Table 1. Minimum/Maximum/Average root mean squared axis fitting errors between the expert annotations and the fitting approaches on ten sample roots. (GKS = gray-value based kernel smoothing, PKS = surface point based kernel smoothing, CCM = the proposed coupled curve model)

	Expert 2	GKS	PKS	CCM
	min/max/avg [μm]	min/max/avg [μm]	min/max/avg [μm]	min/max/avg [μm]
Expert 1	1.78/5.32/3.09	5.52/17.30/10.68	3.69/16.94/8.46	**3.18**/**11.22**/**6.07**
Expert 2	N/A	6.38/14.66/11.38	**3.37**/17.36/8.65	4.55/**12.65**/**7.32**

Fig. 3(a) (panels 2 and 3). Although the images are gamma corrected, the signal attenuation in z direction is still visible.

To evaluate the axis fits, two experts manually annotated axis points of ten root tips. For this the data sets were first rotated to roughly align the root axis with the Euclidean x-axis. This avoids elliptic distortions of the visible root sections during annotation. Both experts picked the root center at every 100th x-section of the data set guided by a circle of appropriate diameter. The average annotation difference between the experts is $3\mu m$, which is in the order of an average nucleus radius.

We detect the nuclear center positions of a selected tissue layer based on rotationally invariant volumetric gray value features, namely the magnitudes of voxelwise solid harmonic spectra [10]. Based on these features a probabilistic SVM model which was trained on two separate datasets is applied and local probability maxima are used as nucleus candidate positions.

We again compared the CCM to Gaussian kernel smoothing approaches, this time incorporating either the gray values directly (GKS) or the positions of the nuclei (PKS). We chose a kernel width of $40\mu m$ to reach a smooth curve, that still shows good localization properties. The estimated axes on sample roots are shown in Fig. 3. Especially in Fig. 3(a) the bias of GKS towards regions with higher gray values is clearly visible. As already seen in the synthetic results PKS relies on homogeneously distributed points, and therefore on the detector quality. In all samples (Fig. 3(a-c)) the detector reported many false positives in low signal parts of the recording, leading to deformations of the PKS axis estimate towards these points. Also CCM was affected by the false positives in the root volume (Fig. 3(b) (xz panel)) resulting in a slight shift of the model axis. In contrast to PKS, in which the points "attracted" the axis, for CCM false detections in the root interior were explained by an erroneous model shift in the opposite direction.

5 Conclusion

We presented a variational approach to robustly model tubular structures defined by their axis and thickness functions based on sparse and noisy surface point

samples. The approach is able to follow tubes of very complex bending patterns and also allows for moderate thickness variations. When exchanging the tube thickness constancy penalizer by a penalizer on a higher derivative degree, the approach can be adapted to find the axis of arbitrary objects of revolution.

The possibility to introduce arbitrarily many tube seeds into the model allows to simultaneously match all tubes within a data set. Although branching structures are not yet introduced in the model, its capability to simultaneously model multiple tubes in a data set in one energy minimization allows to trace the single branches up to the branching point.

Acknowledgements

We thank the members of our team for helpful comments on the manuscript. We also gratefully acknowledge the excellent technical support from Roland Nitschke (ZBSA). This work was supported by the DFG, the Excellence Initiative of the German Federal and State Governments (EXC 294), European Space Agency, Bundesministerium für Bildung und Forschung (BMBF), Deutsches Zentrum für Luft und Raumfahrt, and the Freiburg Initiative for Systems Biology (FRISYS).

References

1. Bauer, U., Polthier, K.: Generating parametric models of tubes from laser scans. Computer-Aided Design 41(10), 719–729 (2009)
2. de Boor, C.: A practical guide to splines, Applied Mathematical Sciences, vol. 27. Springer-Verlag, 3rd edn. (1978)
3. Friman, O., Hindennach, M., Kühnel, C., Peitgen, H.O.: Multiple hypothesis template tracking of small 3d vessel structures. Med. Image Anal. 14, 160–171 (2010)
4. Kirbas, C., Quek, F.: A review of vessel extraction techniques and algorithms. ACM Comput. Surv. 36(2), 81–121 (2004)
5. Laptev, I., Mayer, H., Lindeberg, T., Eckstein, W., Steger, C., Baumgartner, A.: Automatic extraction of roads from aerial images based on scale space and snakes. In: Machine Vision and Applications. vol. 12, pp. 23–31 (2000)
6. Lee, I.K.: Curve reconstruction from unorganized points. Computer Aided Geometric Design 17(2), 161–177 (2000)
7. Meijering, E., Jacob, M., Sarria, J.C., Steiner, P., Hirling, H., Unser, M.: Design and validation of a tool for neurite tracing and analysis in fluorescence microscopy images. Cytometry Part A 58A(2), 167–176 (2004)
8. Pock, T., Beichel, R., Bischof, H.: A novel robust tube detection filter for 3d centerline extraction. In: Proc. SCIA. vol. 3540, pp. 481–490 (2005)
9. Schnabel, R., Wahl, R., Klein, R.: Efficient ransac for point-cloud shape detection. Computer Graphics Forum 26(2), 214–226 (2007)
10. Skibbe, H., Reisert, M., Ronneberger, O., Burkhardt, H.: Increasing the dimension of creativity in rotation invariant feature design using 3d tensorial harmonics. LNCS 5748/2009, 141–150 (2009)
11. Wang, Q., Ronneberger, O., Burkhardt, H.: Using lateral coupled snakes for modeling the contours of worms. LNCS 5748/2009, 542–551 (2009)